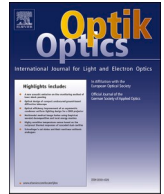




ELSEVIER

Contents lists available at ScienceDirect

Optik

journal homepage: www.elsevier.com/locate/ijleo

Original research article

Physical-based methodology for prediction of weld bead characteristics in the Laser Edge Welding process

Seyedeh Fatemeh Nabavi^a, Mohamad Hossein Farshidianfar^a,
Anooshiravan Farshidianfar^{a,*}, Behrooz Beidokhti^b

^a Mechanical Engineering, Engineering department, Ferdowsi University of Mashhad, Mashhad, Iran

^b Material and Metallurgical Engineering, Engineering department, Ferdowsi University of Mashhad, Mashhad, Iran



ARTICLE INFO

Keywords:

Physical-based methodology
Laser edge welding
Weld properties
Physical parameters
Combined physical parameter

ABSTRACT

A comprehensive physical-based methodology is introduced to predict weld bead properties in the Laser Edge Welding (LEW) process. Laser edge welding of AISI 316L stainless steel thin sheets are conducted to investigate the behavior of geometrical, mechanical and metallurgical properties of the weld bead. The effect of significant processing parameters including the laser power, speed and focal distance are considered. The method however, utilizes a set of physical-based contour plots to predict the trend of weld characteristics using the heat input and power density. A novel combined physical parameter is also introduced and optimized to indicate the exact quantitative effectiveness of each physical and processing parameter. The developed approach is utilized to analyze a broad range of weld bead characteristics. First, weld bead geometrical characteristics such as weld width, penetration and distortion are studied. The physical-based method revealed that the power density has a significant effect on the weld penetration-to-width ratio while distortion is governed by the heat input. Variations of the fracture load are analyzed based on the corresponding combined parameter. Interestingly, a greater penetration-to-width ratio results in a higher fracture load. Finally, microstructural evolutions are investigated in three main regions, including the top, middle and bottom of the weld bead. A skeletal ferrite phase is observed in the mid-zone, which increases with increase of power density. The presented methodology can be applied to a broad range of other laser materials processing techniques to obtain insightful process design tips in order to achieve tailor-made properties.

1. Introduction

Laser Edge Welding (LEW) involves applying the laser as a heat source to construct a bond between materials. LEW constructs a weld zone on the intersection of materials that is heated and cooled rapidly, resulting in very fine microstructures and strong joints. Power density involved in LEW is an order of magnitude larger compared to conventional welding techniques. LEW has several advantages such as small heat affected zone [1,2], high speed production [3] and controlled energy input and localized melting [4]. Since the laser welding technology is novel, in-depth study of all its major weld configurations has yet to be addressed in literature. One of the most important laser welding configurations is the LEW process, which is implemented widely for joining of thin sheets in plate heat exchangers and the aerospace industry. However, very limited research has been conducted on the LEW process and its overall

* Corresponding author.

E-mail address: Farshid@um.ac.ir (A. Farshidianfar).

<https://doi.org/10.1016/j.ijleo.2021.166917>

Received 3 March 2021; Accepted 9 April 2021

Available online 23 April 2021

0030-4026/© 2021 Elsevier GmbH. All rights reserved.

Nomenclature

d	Diameter of the beam
D	Weld deviation of distortion
f	Laser focal distance
F	Weld fracture load
FZ	Fusion zone
HAZ	Heat affected zone
HI	Heat input
p	Laser power
P	Weld penetration
PD	Power Density
PW	Penetration-to-width ratio
v	Laser speed
W	Weld width
m	Power density factor
n	Heat input factor
α	Laser power factor
β	Laser speed factor
γ	Laser focal distance factor

characteristics.

Every weld produced by a LEW process has three main properties that require to be tailored to desired values; (1) geometrical properties, (2) mechanical properties and (3) metallurgical properties. The goal is to produce a weld with desired geometrical, mechanical and metallurgical properties. In fact, these are the most important output parameters of the LEW process. The geometrical design features of a weld include weld distortion, penetration and width. Mechanical and metallurgical characteristics such as fracture load and microstructure are output parameters that define applications and limitation of a weld. Researchers often have extreme difficulty optimizing the LEW process for specific and different applications. Often it requires extensive time-consuming and expensive experimentation to be able to control the weld characteristics under different processing conditions. Understanding the behavior of weld characteristics and effective input parameters will help in the development of an optimized LEW process, capable of producing tailored properties for welds with less experimentation and much faster.

Since, all laser material processing technologies including LEW have specific input parameters, the initial step towards achieving a fully controlled weld property is to understand the effective input physical parameters. Weld output such as geometry, mechanical behavior and metallurgical properties are determined by the manner which the weld energy is applied to the joint [5]. It is known that input energy is controlled by physical parameters. Physical parameters are the combination of processing parameters such as laser power, speed and focused spot size.

Benyounis et. al [6] used response surface methodology to predict laser butt-welding geometry parameters such as penetration, width and heat affected zone's width. The input processing parameters such as laser power, speed and focal position were used in linear and quadratic polynomial equation to predict geometry of weld-bead of medium carbon steel. They realized that increasing speed leads to reduction of penetration, width and HAZ of weld-bead whereas; increase of laser power provides bigger geometry of weld-bead. However, their model was based on a specific range of processing parameters. Thus, it was restricted for a limited region of processing parameters. They used the same methodology to predict mechanical properties of laser butt-weld instead of geometry parameters of weld-bead in another study [7]. The mechanical properties which they considered were tensile strength and impact strength. Similar limitation was observed in their mechanical model in which it was varied for the speed (35,68) cm/min, laser power (1.03,1.37) kW and focal distance (-1,0) mm. Zhang [8] investigated effect of laser butt welding processing parameters on weld parameters of 12 mm thickness stainless steel sheets. The weld parameters which they considered were weld bead geometry, the microstructure and mechanical properties of weld. They pointed out the significant effect of focal position in butt welding of thick plates. They used a range of speed in order to achieve full penetration weld, whereas no model was introduced in their study. Liu et al [9]. provided an optimal design for the dual butt laser welding process of stainless steel 316L using artificial neural networks (ANN) and genetic algorithm (GA). The goal of this optimization was to reduce the number of porosities during the welding process using the Taguchi approach. However, the proposed model could not predict geometry or mechanical properties of the weld-bead. Thus, it can be concluded that all the previous models were based on laser welding processing parameters including power, speed and focal distance. This leads to all models being limited to a restricted range of processing parameters. Thus, it is not possible to apply them in a global process window. To overcome this shortcoming, the model should be based on physical parameters, which can interpret a global understanding of the weld process.

Distortion of thin sheets is one of the challenges of LEW which few studies have addressed. Kim et al [10]. provided an in-depth study of the effect of heat input ratio on distortion of laser-arc welding. Their results indicated that increase of heat input leads to greater bead-on-plate deformation. Their model predicts distortion of bead-on-plate weld as a function of heat input ratio of hybrid welding. However, the model restricted to laser hybrid welding. Hence, just one physical parameter, heat input, was considered in

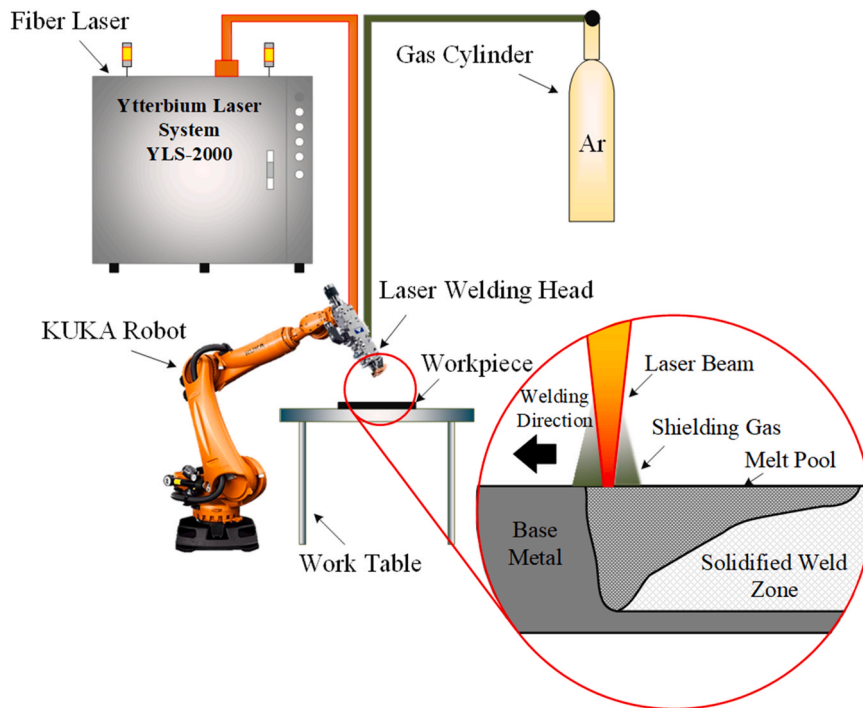


Fig. 1. Schematic of laser machine setup.

their model. The distortion of laser butt-welds of stainless steel 301 was studied by Huang et. Al [11]. With a numerical model, they showed distortion increases by increase of laser heat input. Nonetheless no analytical model was introduced in their study. To our knowledge, there is no study currently available in literature that addresses the distortion of the LEW process, while minimizing distortion is one of the most important design outcomes during a welding procedure.

LEW of thin sheet metals is used in different applications such as Plate Heat Exchangers [12] and electrical motor components [13]. Markovits et al [13], investigated pulsed laminated LEW on 0.5 mm electrical steel sheet. They showed increasing welding speed decreases weld depth and width. Based on their study, the pulse energy and time effects on the width less than depth. However, the effect of laser focal distance and mechanical or metallurgical properties of weld were not considered in their study. Caiazzo et. al [14], provided a study on LEW of 0.7 mm thin Inconel 625 sheet. They pointed out that choosing low heat inputs leads to decrease in the grain size which provides better mechanical properties. Besides, their results noticed growing heat input leads to increasing content of porosity. However, they just considered two processing parameters including speed and power. Similarly, the effect of focal distance and distortion of weld were not studied.

Although LEW have variety of applications, few studies have been focused on it. These related researches were very limited which considered specific processing parameters such as laser power and speed or partial weld properties such as weld penetration, width and microstructure. Another problem is lack of a model for LEW which covers global area with meaningful definition. Moreover, stainless steels which is one of the most beneficial materials due to its corrosion resistance [15] is not studied in LEW research. Therefore, a comprehensive study which considers all the effective parameters and geometrical, mechanical and metallurgical properties of edge weld based on physical parameters is required.

The main objective of this paper is to develop a novel physical-based methodology for integrated prediction of geometrical, mechanical and metallurgical properties of the LEW process. This methodology interprets weld characteristics using a combined set of physical parameters. The approach has two main advantages; firstly, it can be used for a broad range of processing parameters without any limitation, secondly, it provides a physical insight into the LEW process and the effect of different processing conditions on final characteristics. To achieve this goal, three effective processing parameters including laser power, speed and focal distance are considered. A set of experiments are conducted on thin sheet AISI 316L stainless steels to investigate variation of weld bead properties with respect to different LEW processing conditions. Geometrical, mechanical and metallurgical properties of the weld bead are measured and studied in great detail. These characteristics include the weld width, penetration, distortion, fracture load and microstructure. A general approach is introduced to study variations of the weld bead characteristics based on physical parameters instead of processing parameters. In the proposed approach, a set of physical-based contour plots are developed for providing meaningful insights into how weld bead properties are transformed. Furthermore, a unique combined physical parameter is tuned for each weld property to identify the effectiveness level of different input parameters on developing the property. The presented physical-based methodology is a comprehensive tool for analyzing and optimizing of not only the LEW process but also a broad range of other laser materials processing procedures.

Table 1
The selected specimens.

Sample number	p (W)	v (mm/s)	f (mm)
1	1600	35	50
2	1600	30	50
3	1600	25	50
4	1600	30	40
5	1750	30	50
6	1750	25	40
7	1900	35	50
8	1900	30	50
9	1900	35	40

Table 2
Stainless steel 316L chemical composition (wt%).

Cr	Ni	Mo	Mn	Si	C	P	S	Fe
17.0	12.0	2.5	1.5	0.5	0.03	0.03	0.05	Balance

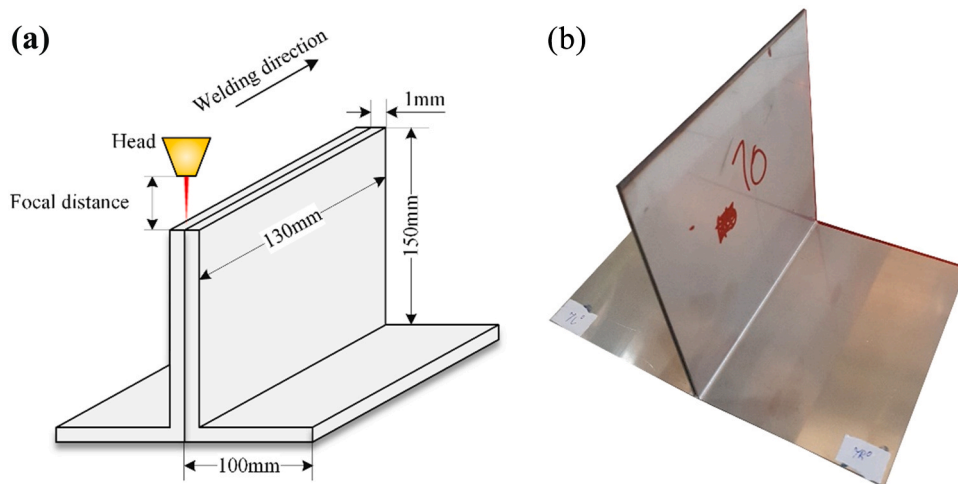


Fig. 2. The LEW; a) Schematic of process condition, b) The welded specimen.

2. Experimental procedure

2.1. Experimental setup

The experimental setup used in the current research for conducting the LEW experiments includes a high power 2 kW Fiber laser, which provides the energy for the welding (Fig. 1). A welding head with 125 mm collimating focal length and 300 mm focusing focal length provides the focused laser beam. The welding motion is provided by a Kuka robot in which the substrate is kept in stationary position and the laser head is moved by the robot arm. Argon shielding gas is supplied on the substrate to prevent oxidation. Therefore, the workpiece is heated by laser beam and melt pool is formed along the edge joint by moving the laser head.

2.2. Design of experiment

The aim of the present study is to develop a generalized methodology for predicting weld properties during the LEW process. Since these properties are influenced by processing parameters, a wide variation of the processing parameters is considered in the current research. Laser power (p), speed (v) and focal distance (f), which are the three most effective processing parameters of the LEW process are considered for experimentation. Variation of processing parameters are studied through nine different specimens in the current research, which are listed in Table 1. The experiments are conducted in three levels of laser power, namely 1600, 1750 and 1900 W. At each level, the welding speed (25–35) mm/s and focal distance (30,50) mm are varied accordingly.

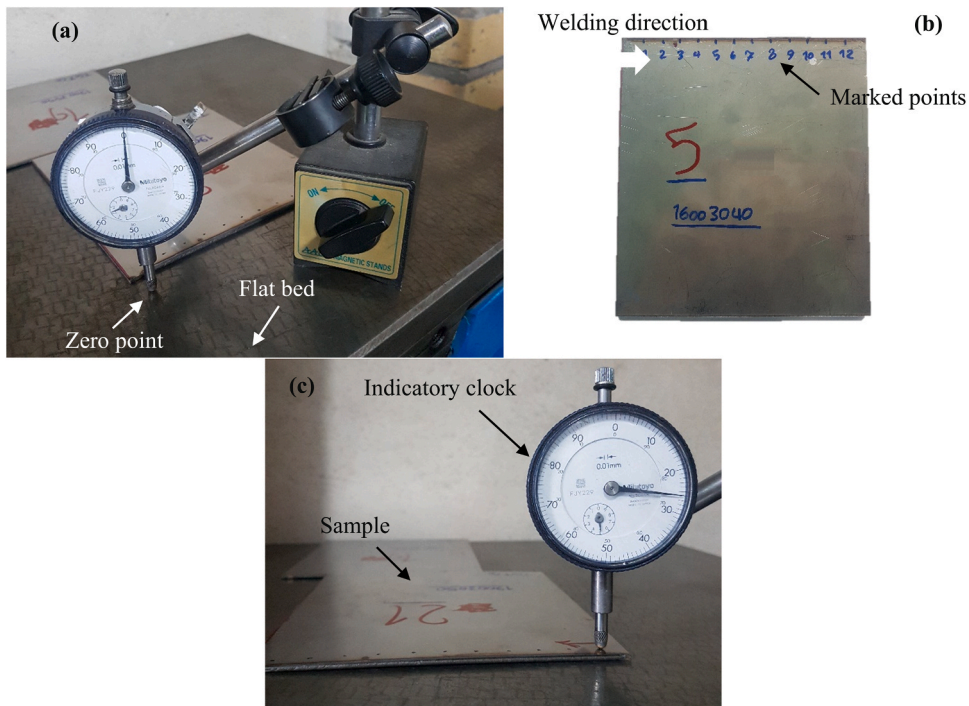


Fig. 3. Distortion measurement process; a) Calibration with zero point of flat bed, b) Marked points of specimen, c) First position of specimen.

2.3. Material preparation and testing procedures

Stainless steels is one of the most beneficial materials due to its corrosion resistance [15]. AISI 316L stainless steel sheets with a thickness of 1 mm and chemical composition shown in Table 2 are used in the current experiments. All AISI 316L sheets were cut into $130 \text{ mm} \times 250 \text{ mm} \times 1 \text{ mm}$ specimens and then bent 90° shown in Fig. 2(a). The specimens were clamped along the intersections to ensure a no-gap region along the edge. Prior to the LEW process, all specimens were rinsed with water and washed with alcohol to remove any contamination.

In order to analyze microstructure properties, specimens were prepared using SiC grit paper with grit sizes ranging from 360 to 2000, and later polished with alumina powder. The specimens were etched in Glyceregia etchant for macrography tests to reveal weld width and penetration. Oxalic acid 10% etchant was used for metallography test to analyze the microstructure. The microstructure was analyzed using optical microscopy with imaged obtained using an IMM420 microscope. Mechanical properties including the fracture load were measured by the T-peel test based on ASTM D1876 [16].

After the LEW process, the specimens were sectioned by water jet for geometrical, mechanical and microstructural examination (Fig. 2(b)). The distortion produced along the weld bead during LEW process was measured by the indicatory clock Mitutoyi FJY229. The clock was put on the flatbed to calibrate a zero point. Each weld edge was marked into 1 cm regions as shown in Fig. 3(a). The height of each marked point was measured by the indicatory clock as shown in Fig. 3(b). It should be noted after finishing the measurement of each specimen, the indicatory clock was put on the flatbed to ensure the correctness of calibration. Moreover, the flatness of all specimens before welding was measured to ensure that the measured distortion was a result of the LEW process.

3. Physical-based methodology

Change of processing parameters, leads to variation in weld bead properties. To understand and predict these properties models are required. Most models however, are based on processing parameters, which possess two main challenges. Firstly, they are restricted to a narrow and local range in which experiments are conducted. Secondly, they do not provide physical insight into the process. Therefore, a more general modelling approach is required to provide an in-depth physical meaning of the process. Models based on physical rather than processing parameters can overcome the above-mentioned shortcomings.

For the current study, two physical parameters including the heat input (*HI*) [14] and power density (*PD*) [17] are considered for analyzing the LEW process. The heat input and power density formulations are provided as follows:

$$HI = p/v [\text{J}/\text{mm}] \quad (1)$$

$$PD = p/a [\text{w}/\text{mm}^2] \quad (2)$$

Table 3
The results of geometry analysis of specimens and their physical parameters.

Parameter→ Specimen↓	HI (J/mm)	PD (W/mm ²)	W (μm)	P (μm)	PW (%)	D (μm)
1	45.71	9.57×10^2	1980	1297	65.50	14.40
2	53.33	9.57×10^2	1932	1166	60.35	17.80
3	64.00	9.57×10^2	1646	1013	61.54	121.00
4	53.33	1.39×10^3	1719	1426	82.95	14.40
5	58.33	1.04×10^3	1932	1221	63.19	112.30
6	70.00	$1.52e \times 10^3$	1098	1145	104.28	120.70
7	54.28	$1.13e \times 10^3$	1813	1132	62.43	37.10
8	76.00	$1.13e \times 10^3$	1868	1515	81.10	218.60
9	54.28	$1.65e \times 10^3$	1519	1370	90.19	over

in which p , v and a define the laser power, speed and spot size area, respectively. The heat input (HI) defines the amount of energy deposited per unit length during the LEW process [14]. On the other hand, the density of power, which radiates on a specific area (a) is interpreted by power density (PD) [18]. These physical parameters take into account the effect of three input processing parameters simultaneously. Therefore, they provide a much more broader understanding of the LEW process compared to single processing parameters. The heat input and power density of all nine specimens are reported in Table 3.

While physical parameters such as the heat input and power density are required to understand the characteristics of an LEW process, it is beneficial to combine these parameters into a single compact form to develop a more general and straightforward framework. Such a compact form can be defined in terms of a new combined parameter. In the current methodology, a unique combined parameter (CP) is considered in the following form:

$$CP = HI^n PD^m \quad (3)$$

in which HI and PD define the heat input and power density, and n and m define the degree of importance for each of these physical parameters, respectively. Eq. (4) can also be represented in terms of input process parameters accordingly:

$$CP = p^\alpha v^\beta f^\gamma \quad (4)$$

in which α , β and γ are constant parameters that demonstrate order of importance for each input processing parameters including the laser power, speed and focal distance, respectively. Under the current methodology, the constant values n and m , are calculated based on a correlation between the CP value and a specific output property. In other words, each weld bead property is defined as a function of the combined parameter as follows:

$$\text{Weld Bead Properties} = f(CP) + \text{Error} \quad (5)$$

Using general optimization techniques, optimized n and m values are calculated to minimize the error (or root mean square of the error) value. A more detailed explanation is provided in the Appendix.

The developed physical-based methodology is implemented in two main stages to analyze the output property of any laser welding procedure:

1. A set of 2D physical-based contour plots are constructed describing each specific characteristic (e.g. weld width, penetration, distortion or fracture load) based on the heat input and power density. These contour plots provide a comprehensive perspective on how each characteristic is transformed through heat input and power density changes.
2. The unique combine parameter (defined in Eq. (3)) is optimized for each output characteristic to predict these characteristics based on a single parameter rather than multiple ones. The optimized constants n , m , α , β and γ are compared and analyzed to define the effective role of different physical and process parameters on the weld characteristic.

In the current study, the output characteristics of the LEW process will be analyzed based on physical parameters and the described combined parameter in order to gain a detailed insight into the process.

4. Results and discussion

Geometrical, mechanical and metallurgical characteristics such as weld width, penetration, distortion, fracture load and microstructure are output parameters that define weld bead properties. An inclusive understanding of the effect of different input physical parameters on final properties will assist in the development of an optimized LEW process, capable of producing tailor-made properties. Results of geometrical, mechanical and microstructural measurements of the weld specimens discussed in Section 2 are presented in the following sections. More importantly, the physical-based methodology described in Section 3 is implemented to analyze the weld bead characteristics and how they are formed.

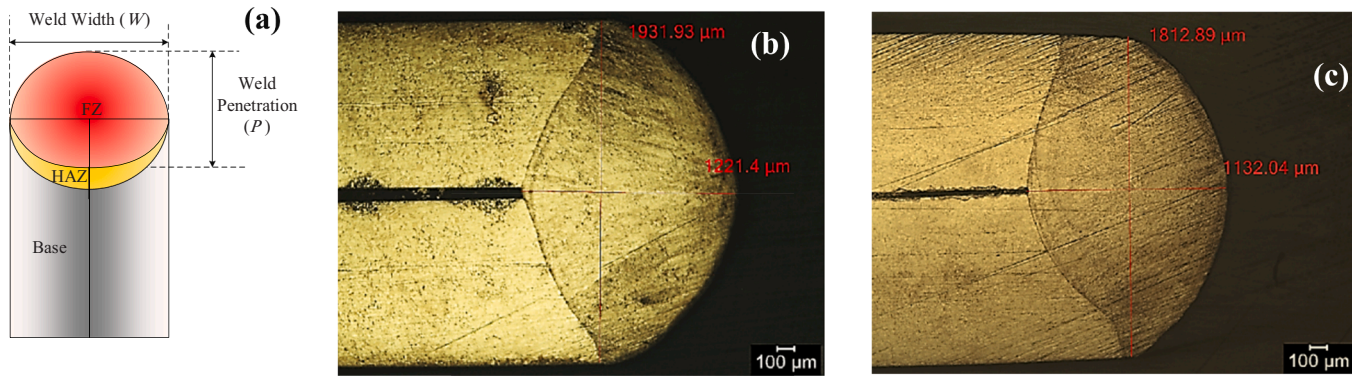


Fig. 4. The specimen of LEW a) Schematic, b) The microscopic picture X40 of specimen 4, c) The microscopic picture X40 of specimen 6.

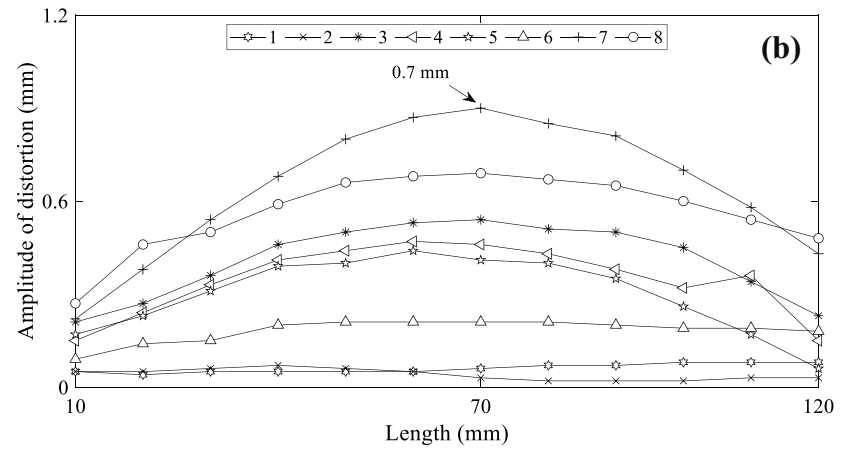
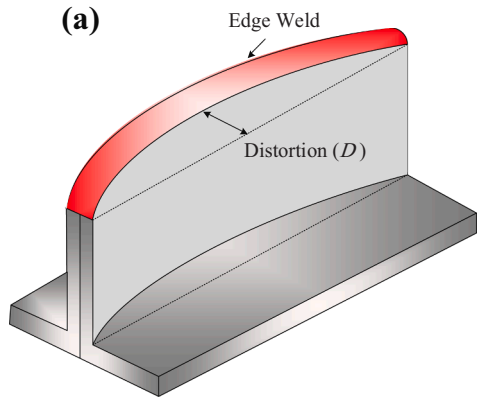


Fig. 5. The distortion of specimen, a) Schematic, b) Measured values versus welding bead length.

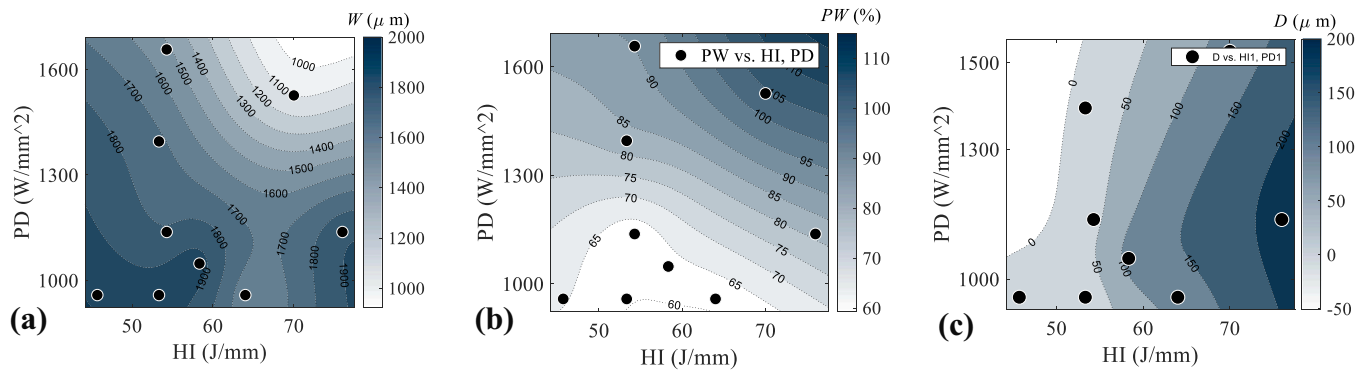


Fig. 6. The contour plot of weld bead geometry; **a)** Weld width, **b)** PW ratio and **c)** Distortion versus power density (W/mm^2) and heat input (J/mm).

Table 4

The constants of combined parameter for geometrical properties of weld bead including weld width, penetration-width ratio and distortion.

CP parameters→ Weld properties↓	n	m	α	β	γ
W	4.7	6	10.7	-4.7	-6
PW	1	2	3	-1	-2
D	4.2	-1	3.2	-4.2	1

4.1. Weld bead geometrical properties

4.1.1. Weld width and penetration

It is highly important to achieve specific geometrical features in a welding process. Different geometrical features of a weld bead can be investigated. However, the two most significant features are the weld width (W) and weld penetration (P), which are shown schematically in Fig. 4. Considering the fusion (FZ) and heat affected zones (HAZ), the weld width is defined as the width of the fusion zone, whereas the weld penetration is the height of the fusion zone. The weld penetration-to-width ratio (PW ratio) is another important geometrical feature expressed as the ratio of weld penetration to weld width. As an example, the measured weld width and penetration for specimens 4 and 6 are shown in Fig. 4(b) and (c) respectively. The measured weld width, penetration and penetration to width ratio of all nine specimens are reported in Table 3. No direct correlation is observed between the physical parameters (heat input and power density) and weld width or penetration based on this table. Nonetheless, it can be generally stated that a combination of these two parameters governs the geometrical features of a weld.

4.1.2. Weld distortion

Distortion is a negative outcome of any welding process. Minimizing and controlling welding distortion is of critical importance, specifically during welding of thin sheet metals. In applications such as welding of plate heat exchangers, which includes welding of 0.5–1 mm thin sheet metals, welding distortion leads to assembly issues. Hence, analysis and optimization of distortion in the LEW process is of significant importance. To further investigate geometrical features of the weld bead, longitudinal distortion of specimens was measured as shown in Fig. 5(a). The distortion of each specimen is plotted along the weld length in Fig. 5(b). It should be noted that the distortion of specimen 9 was very large and could not be measured.

According to Fig. 5(b), distortion profile of all specimens are in the form of a semi-quadratic profile. In specimens 1, 2 and 4, the values of distortion are very small, thus the profile cannot be captured. This semi-quadratic profile is in agreement with a previous study, which analyzed longitudinal distortion of the laser butt welding process [11]. The high-power laser beam produces a thermal strain in weld specimens, which provides distortion. Because of clamping at both start and end of specimens, thermal strain is guided to central part where is free to distort. Therefore, it is predictable to observe maximum values of distortion at the center of specimen.

In order to compare the deformation of different processing condition in detail, a quantitative parameter of weld bead distortion is required. Deviation of the distortion profile (D) defines the spread of the weld bead distortion about its mean value. A higher D value indicates a more distorted welding process. Therefore, deviation provides a suitable quantitative representation of each weld specimen distortion. The weld distortion deviation (D) of all specimens is calculated and reported in Table 3.

4.1.3. Physical-based analysis of geometrical properties

A set of physical-based contour plots were designed to investigate the effect of physical parameters on weld bead geometry properties. Contour plots of the weld width, penetration and distortion as a function of the heat input and power density are plotted in Fig. 6. These plots have been fitted in MATLAB with an R-squared of 1 (R-squared is the percentage of the dependent variable variation that a linear model explains).

As can be seen in Fig. 6(a), power density (PD) and heat input (HI) are equally effective on the weld width (W). Increase of PD and HI leads to a narrower weld width, which is in agreement with the physical characteristics of the LEW process. The higher power density and heat input provides a more concentrated energy resulting in a decreased weld width.

According to the contour plots shown in Fig. 6(b) and (c), the penetration-to-width ratio (PW) and welding distortion (D) are mostly governed by only one of the two physical parameters. Fig. 6(b) shows a horizontal contour; indicating the critical role of power density in defining the PW ratio. Accordingly, at a constant power density, the penetration-to-width of a weld remains consistent regardless of the amount of heat input. This is specially the case at lower heat inputs ($HI < 60$ J/mm). On the other hand, the weld distortion shown in Fig. 6(c) is dominated by the heat input. According to this contour plot, specimens having the same heat input have exactly the same distortion values regardless of the amount of their power density. In other words, the distortion of an LEW process is invariant with respect to power density changes while the heat input is remained unchanged. Fig. 6(c) also reveals that heat inputs higher than 60 J/mm are not recommended since they result in distortion deviations of over 100 μm . Specimens with lower heat inputs however, have distortions less than 40 μm . Therefore, to control distortion in the LEW process, one has to limit the heat input to lower than 60 J/mm. The physical-based contour plot analysis shown in Fig. 6, provides an extremely operational tool for understanding and optimizing geometry characteristics of the LEW process.

According to the proposed methodology, a combined physical parameter (CP) (defined in Eqs. (3)–(4)) can be optimized for every output characteristic. Such a parameter provides a simplified prediction for each characteristic based on a single physical-based parameter instead of multiple parameters. Moreover, it justifies the respective role of each physical parameter stated above. A combined parameter (CP) was optimized based on each of the three geometrical properties based on the optimization method describe

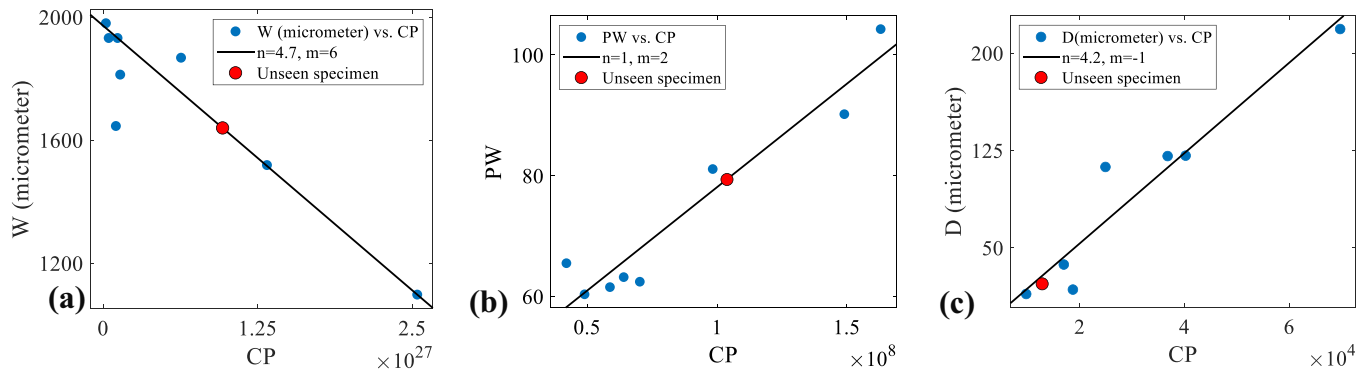


Fig. 7. The combined parameter versus experimental results for different weld bead geometry properties including; a) Width, b) PW ratio and c) Distortion.

Table 5
The experimental and predicted values of weld properties for test specimen.

Weld properties	Experimental	Predicted	Error (%)
W (μm)	1719	1639	- 4.61
PW	82.95	79.37	- 4.32
D (μm)	14.40	22.23	+ 54.37

Table 6
The results of mechanical analysis of specimens and their physical parameters.

Parameter→ Specimen↓	PD (W/mm^2)	HI (J/mm)	F (kN)
1	9.57×10^2	45.71	4.03
2	9.57×10^2	53.33	5.23
3	9.57×10^2	64.00	5.55
4	1.39×10^3	53.33	5.85
5	1.04×10^3	58.33	5.70
6	1.52×10^3	70.00	6.54
7	1.13×10^3	54.28	4.84
8	1.13×10^3	76.00	5.87
9	1.65×10^3	54.28	8.08

in Section 3 (Eq. (5)). The calculated *CP* constants (such as n , m , α , β and γ) are presented in Table 4. The weld width, penetration-to-width ratio and distortion are plotted as a function of the *CP* parameter in Fig. 7.

The data point of one of the nine specimens was not used for the optimization process (indicated by “Unseen specimen” in Fig. 7), so that it would be later used for verification purposes. Processing parameters of the unseen specimen were $p = 1600$ W, $v = 30$ mm/s and $f = 40$ mm. The experimental and predicted values of the weld bead geometrical properties for the unseen specimen are provided in Table 5. The combined physical parameter (*CP*) provides an accurate prediction of geometrical properties for the unseen specimen (except for distortion), which verifies the physical-based analysis methodology. The general accuracy of this approach is also evident in Fig. 7, since the data points for all three geometrical characteristics are very close to their fitted lines.

Significant conclusions can be made from the optimized *CP* coefficients (n , m , α , β and γ) presented in Table 4. According to Eq. (3), coefficients n and m define the level of importance of the heat input and power density, respectively. A larger n coefficient indicates a more effective role for the heat input in determining the specified weld bead property, whereas a larger m indicates a more effective role for the power density. The same is true for coefficients α , β and γ , which define the level of importance of the laser power, speed and focal distance, respectively. Comparing n and m values in Table 4, it is inferred that heat input and power density are as equally effective on the weld width (nearly equal n and m values, $m = 1.27n$). Yet the penetration-to-width ratio is governed by the power density (m is double the value of n , $m = 2n$), and distortion is significantly governed by the heat input (n value is four times the value of m , $n = 4.2m$). Overall, the *CP* parameter and its coefficients provide a systematic and quantitative analysis of the physical-based contour plots presented in Fig. 6.

In addition, the α , β and γ coefficients of the *CP* parameter reported in Table 4 outlines the effect of processing parameters on geometrical properties. Surprisingly, the laser power is the most effective processing parameter among the three main parameters; having the largest value for both the weld width ($\alpha = 10.7$) and penetration-to-width ratio ($\alpha = 3$). Results suggest that distortion is mostly governed by the laser speed and power, while the focal distance has a very minimal effect.

4.2. Weld bead mechanical properties

Fracture load is a critical mechanical property of the weld bead, which represents the strength of a welding joint. Maximizing the fracture load is beneficial for ensuring persistence against external forces. A reduced weld fracture load in the LEW process leads to failure in products such as plate heat exchangers, which are under high hydrostatic pressure. Therefore, optimizing and predicting the fracture load of a weld is of considerable importance. The measured fracture load (F) of all nine specimens are provided in Table 6.

4.2.1. Physical-based analysis of mechanical properties

It is difficult to find a quick positive correlation between physical parameters (heat input and power density) and the weld fracture load in Table 6. To understand the behavior of weld mechanical property, physical-based contour plots of the fracture load are mapped as a function of physical parameters in Fig. 8(a). As can be seen in this figure, increase of both power density (*PD*) and heat input (*HI*) lead to an increase of the fracture load. It is observed that at high power densities or heat inputs ($PD > 1300$ W/mm^2 or $HI > 55$ J/mm) the effect of heat input on the fracture load is negligible. In Table 6, specimens 3, 4 and 7 illustrate this point clearly. The fracture load of these specimens is in the same range (from 5.55 to 5.87 kN), whereas their heat inputs vary significantly (from 58 to 76 J/mm). These specimens have the same fracture load only because of their similar power density values.

To investigate the effect of physical parameters on the fracture load quantitatively, the optimized combined parameter is plotted in Fig. 8(b). The calculated *CP* constants (such as n , m , α , β and γ) for the weld fracture load are reported in Table 7. The predicted values of the unseen specimen are also provided in this table, which validate the optimization process.

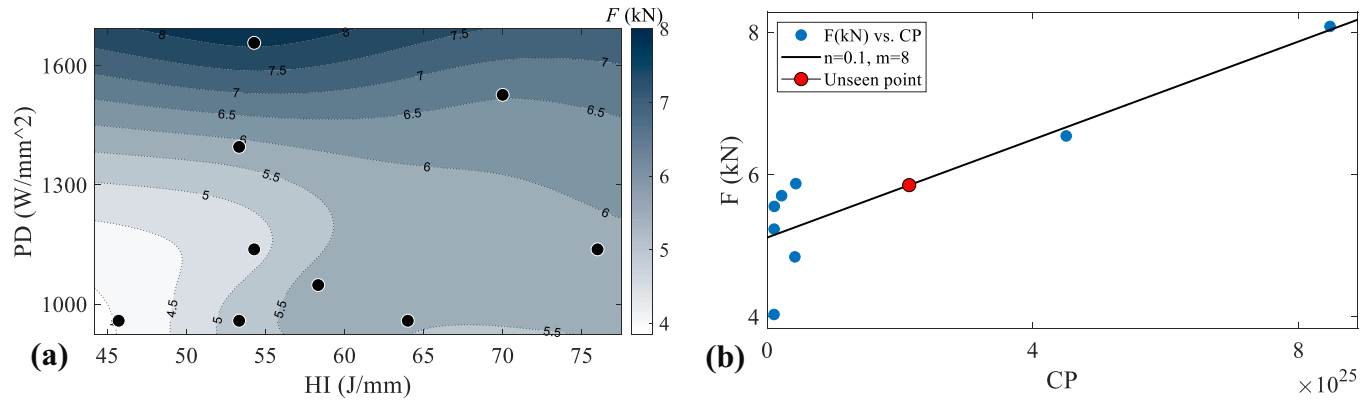


Fig. 8. The effective physical parameter on weld fracture load; a) F versus HI , b) F versus PD .

Table 7
Parameters of $CP = HI^n PD^m = p^\alpha v^\beta f^\gamma$ for different weld properties.

CP parameters	n	m	α	β	γ
	0.1	8	8.1	-0.1	-8
Weld properties	Experimental		Predicted		Error (%)
F (kN)	5.85		5.83		0.39

Interesting results can be deduced from the CP constants provided in Table 7. First, the fracture load is significantly dominated by power density since m has a much larger value compared to n (m is 80 times bigger than n , $m = 80n$). This conclusion is in agreement with the physical-based contour plots shown in Fig. 8(a). Second, the laser speed is the least effective processing parameter on the fracture since β is much smaller than α and γ . Therefore, to produce a weld with high fracture load, it is recommended to increase the power density by increasing the laser power and reducing the focal distance. The results obtained from the CP constants are extremely beneficial in designing insightful weld procedures for the LEW process.

4.2.2. Correlation between mechanical and geometrical properties

Since geometrical characteristics of the weld bead can be easily obtained by simple visual inspections, a methodology that can interpret mechanical properties based on geometrical properties is of great value. Therefore, a correlation between mechanical and geometrical properties was analyzed. Fig. 9(a) is a contour plot which defines fracture load as a function of weld width (W) and penetration (P). Increase of weld penetration leads to increase of fracture load while reduction of weld width results in a reduced fracture load. In other words, increase of the weld penetration-to-width develops a higher fracture load as plotted in Fig. 9(b). This figure utilizes the non-dimensional PW ratio to estimate fracture load. These plots provide a suitable non-destructive methodology for predicting the fracture load based on visual measurements of the weld width and penetration.

4.3. Weld bead microstructural properties

Fig. 10 displays the microstructure of the welded joint of specimen 3. The solidification microstructure of fusion zones (FZ) consists of austenite dendrites (light regions) and interdendritic δ -ferrite (dark regions) with both skeleton and lathy morphologies. Three different zones including top, middle and bottom are observed according to Fig. 10 (a–c), respectively. There is a difference in both grain size and growth orientation in above-mentioned zones. Coarse column crystals formed along the heat dissipation direction. At the fusion zone center, the temperature gradient was low and the solidification rate was high; and the planar growth was dominant. From the center to the bottom, the temperature gradient was increased gradually. Therefore, the microstructural morphology was changed from planar to dendritic mode. Also, the lathy ferrite was observed at the fusion line and the microstructure of the center zone contained more amounts of skeleton ferrite. However, the change in the growth orientation at the top of the FZ could be related to the air cooling phenomenon occurred at the top. The above-mentioned three zones were also observed in other specimens.

5. Conclusions

A novel physical-based methodology was developed to analyze and predict weld bead characteristics in the laser edge welding (LEW) process. Using this approach, laser edge welding of AISI 316L thin sheets was studied in order to understand the transformations of the main process outputs. Based on initial studies, the power density (PD) and heat input (HI) were considered as the two main governing physical parameters affecting final geometrical, mechanical and metallurgical properties. Characteristics such as the weld height, width, distortion, fracture load and microstructure were measured and analyzed in detail. A set of physical-based contour plots and unique combined physical parameters were established to explain variations of these properties based on the power density and heat input. The following interesting results were concluded from the developed framework:

- In terms of weld bead geometrical properties, both power density and heat input had an equally influential role in defining the weld width and penetration. Increase of PD and HI led to a narrower weld width. Physical-based contour plots revealed the critical role of power density in defining the penetration-to-width ratio. The weld distortion however, was governed by the amount of heat input during the process. For specimens having similar heat inputs but different power densities, the amount of distortion was the same.
- Analyses on mechanical properties revealed that the weld fracture load is in positive correlation with power density. The overall results indicated that the effect of welding speed is negligible on fracture load. Thus, in order to achieve desired fracture loads it is recommended to change the laser power and focal distance.
- Correlating the weld fracture load with its geometrical characteristics, it was shown that in welds with similar penetration, the specimen with narrower weld width leads to a higher fracture load. On the other hand, when two specimens have the same weld width, the specimen with the deeper weld provides a greater fracture load. The developed mechanical-geometry contour plots provide a suitable non-destructive methodology for predicting the fracture load based on visual measurements of the weld width and penetration.
- Finally, metallurgical analyses of the weld bead indicated an overall austenitic, skeletal ferrite and lathy ferrite structure in the top, middle and bottom regions of the laser edge welding process.

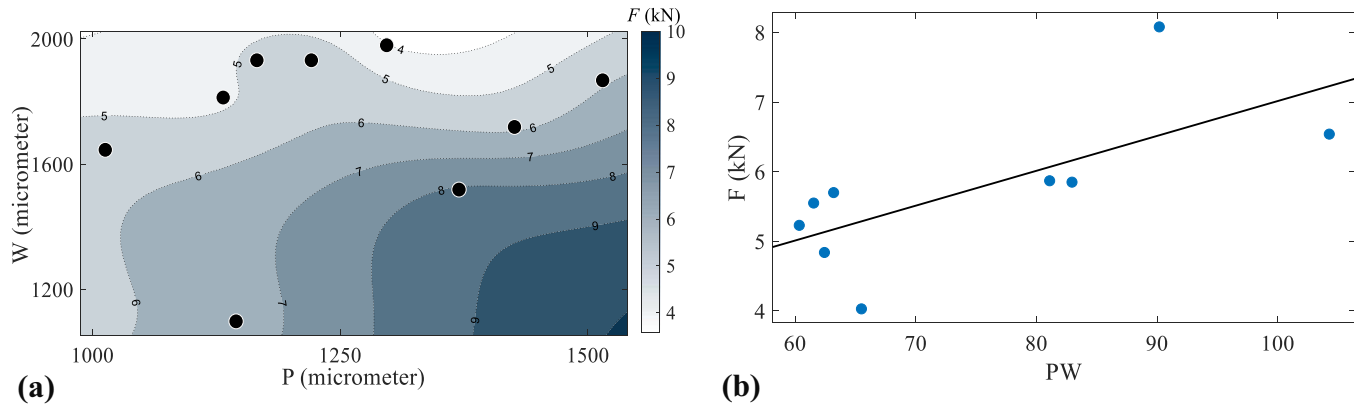


Fig. 9. The fracture load of LEW, a) the contour plot versus weld width and penetration b) versus penetration-to-width ratio.

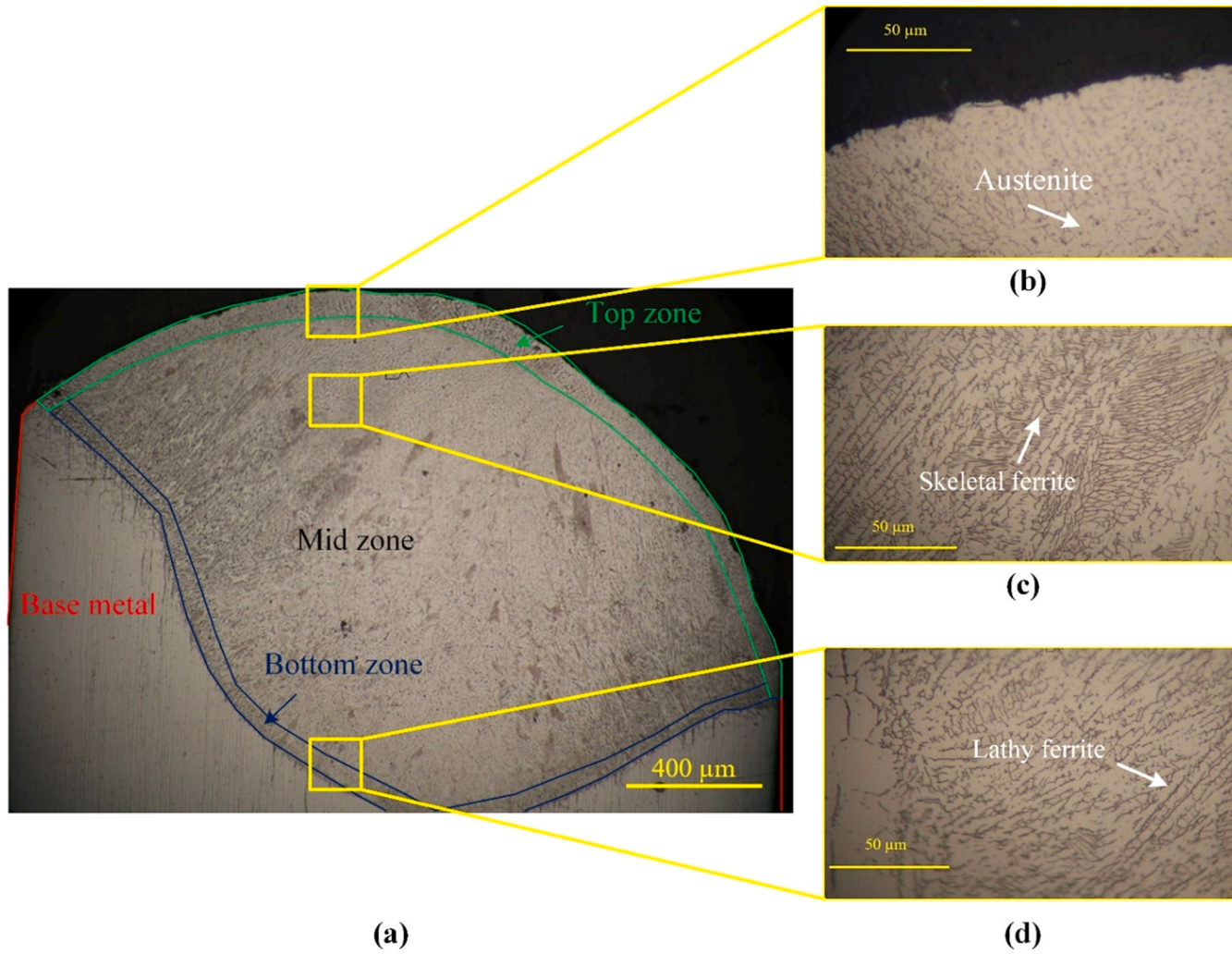


Fig. 10. Specimen 3, a) X100, b) Top-zone (X800), c) Mid-zone(X800), d) Bottom-zone (X800).

Table 8

The constants of presented *CP* for weld width, penetration-to-width ratio, distortion and fracture load.

CP parameters→ Weld properties↓	<i>n</i>	<i>m</i>	<i>P</i> ₁	<i>P</i> ₂
<i>D</i>	4.2	-1	0.003	-16.3
<i>W</i>	4.7	6	-3.44×10^{-25}	1972
<i>PW</i>	1	2	3.42×10^{-7}	43.86
<i>F</i>	0.1	8	3.446×10^{-26}	5.112

A list of significant design tips is achieved using the physical-based approach. The proposed method provides a general framework for optimizing the final properties of a laser edge weld without requiring extensive and time-consuming experimentation.

Funding

Not applicable.

Availability of data and material

Not applicable.

Code availability

Not applicable.

Declaration of Competing Interest

The authors declare that they have no known competing financial interests or personal relationships that could have appeared to influence the work reported in this paper.

Acknowledgment

Firstly, this study was provided under fund support of Taha Ghaleb Toos (TGT) Co. through grant number of LEW: 2020-1-A. A special thanks to TGT Co. because of both spiritual and financial supports during all parts of preparation of presented paper. Secondly, the authors would like to express appreciation to Mr Ali Ehteshami who was good adviser to presented paper.

Appendix

As mentioned, combined parameter (*CP*) presented as $CP = Hl^n PD^m$. To investigate presented methodology with experiment a relation, which also define correlation is defined as Eq. (A).

$$\text{Weld Bead Properties} = P_1 \times CP + P_2 \quad (\text{A})$$

where *P*₁ and *P*₂ are constants, which interpret the slope and intercept of the fitted line. The introduced constants are provided in Table 8.

References

- [1] L. Chen, L. Zhou, C. Tang, W. Huang, C. Wang, X. Hu, J. Wang, F. Yan, X. Wang, Z. Jiang, X. Shao, Study of laser butt welding of SUS301L stainless steel and welding joint analysis, *Int. J. Adv. Manuf. Technol.* 73 (9–12) (2014) 1695–1704.
- [2] M. Moradi, M.K. Moghadam, M. Shamsborhan, Z.M. Beiranvand, A. Rasouli, M. Vahdati, A. Bakhtiari, M. Bodaghi, Simulation, statistical modeling, and optimization of CO₂ laser cutting process of polycarbonate sheets, *Optik* 225 (2021), 164932.
- [3] F. Khodabakhshi, M. Farshidianfar, A. Gerlich, M. Nosko, V. Trembošová, A. Khajepour, Effects of laser additive manufacturing on microstructure and crystallographic texture of austenitic and martensitic stainless steels, *Addit. Manuf.* 31 (2020), 100915.
- [4] M.H. Farshidianfar, F. Khodabakhshi, A. Khajepour, A.P. Gerlich, Closed-loop control of microstructure and mechanical properties in additive manufacturing by directed energy deposition, *Mater. Sci. Eng. A* 803 (2021), 140483.
- [5] D. Petković, Prediction of laser welding quality by computational intelligence approaches, *Optik* 140 (2017) 597–600.
- [6] K. Benyounis, A. Olabi, M. Hashmi, Effect of laser welding parameters on the heat input and weld-bead profile, *J. Mater. Process. Technol.* 164 (2005) 978–985.
- [7] K. Benyounis, A.-G. Olabi, M. Hashmi, Multi-response optimization of CO₂ laser-welding process of austenitic stainless steel, *Opt. Laser Technol.* 40 (1) (2008) 76–87.
- [8] M. Zhang, G. Chen, Y. Zhou, S. Liao, Optimization of deep penetration laser welding of thick stainless steel with a 10 kW fiber laser, *Mater. Des.* 53 (2014) 568–576.
- [9] B. Liu, W. Jin, A. Lu, K. Liu, C. Wang, G. Mi, Optimal design for dual laser beam butt welding process parameter using artificial neural networks and genetic algorithm for SUS316L austenitic stainless steel, *Opt. Laser Technol.* 125 (2020), 106027.

- [10] Y.-C. Kim, M. Hirohata, M. Murakami, K. Inose, Effects of heat input ratio of laser–arc hybrid welding on welding distortion and residual stress, *Weld. Int.* 29 (4) (2015) 245–253.
- [11] H. Huang, J. Wang, L. Li, N. Ma, Prediction of laser welding induced deformation in thin sheets by efficient numerical modeling, *J. Mater. Process. Technol.* 227 (2016) 117–128.
- [12] Y. Zhicheng, W. Lijun, Y. Zhaokuo, L. Haowen, Shape optimization of welded plate heat exchangers based on grey correlation theory, *Appl. Therm. Eng.* 123 (2017) 761–769.
- [13] T. Markovits, J. Takács, Edge welding of laminated steel structure by pulsed Nd:YAG laser, *Phys. Procedia* 5 (2010) 47–52.
- [14] F. Caiazzo, V. Alfieri, F. Cardaropoli, V. Sergi, Investigation on edge joints of Inconel 625 sheets processed with laser welding, *Opt. Laser Technol.* 93 (2017) 180–186.
- [15] M.P. Ryan, D.E. Williams, R.J. Chater, B.M. Hutton, D.S. McPhail, Why stainless steel corrodes, *Nature* 415 (6873) (2002) 770–774.
- [16] ANON.
- [17] E. Assuncao, S. Williams, Effect of material properties on the laser welding mode limits, *J. Laser Appl.* 26 (1) (2014), 012008.
- [18] W.M. Steen, K.G. Watkins, J. Mazumder. *Laser Material Processing*, Springer, London, 2010.